Dynamic Photoelastic Investigation of Interaction of Stress Waves with Running Cracks

A photoelastic study of interaction of stress waves with running cracks is conducted to investigate the influence of crack-wave interaction on crack-propagation behavior and crack branching

by H.P. Rossmanith and A. Shukla

ABSTRACT—Dynamic photoelasticity in conjunction with high-speed photography was utilized in experiments to study the interaction of stress waves with a running crack. Experimental data were analyzed to study the effect of wave scattering about a moving crack tip. The results indicated a strong influence of stress waves on crack-propagation behavior and crack branching.

Introduction

Fracture mechanics in conjunction with dynamic photoelasticity has received considerable recognition in the study of dynamic wave and crack propagation. The phenomenon of crack/wave interaction is of importance in the exploitation of new and profitable energy resources. Of particular significance are the geothermal heat exploitation, oil-shale research and surface and underground-mining operations. Knowledge of crack/wave interaction enables one to optimize fragmentation and consequently reduce the cost of mining operation.

Rock formations found at quarry sites and oil-shale sites form stacks of layered rock with bedding planes and joint sets present. Upon detonation of an explosive, the wave pattern generated in layered media is extremely complicated and running cracks interact with incident and reflected-elastic-wave systems. Depending on the nature of the wave, the crack may accelerate or decelerate during the interaction phase and, in particular situations, crack branching may be induced.

Elastic-wave-propagation problems have been investigated experimentally and analytically in the past and numerous scientific articles and textbooks appear in the literature.[1,2] Reflection, transmission, refraction and diffraction of plane and cylindrical waves have been studied in detail.[3] Transient response of cracks to impact loads and scattering of waves about stationary and moving cracks have been studied theoretically by Chen and Sih.[4] An experimental photoelastic investigation concerning the interaction between a stationary crack and an impinging dilatational wave is due to Smith.[5] But experimental and analytical research in dynamic crack-wave interaction is rather limited.

This study focuses attention on the dynamic interaction between running cracks and stress waves impinging in a direction normal, tangential and oblique to the prospective crack-propagation plane. Photoelastic-fringe patterns obtained by dynamic photoelasticity in conjunction with high-speed photography are analyzed and discussed. The influence of the transient oscillating stress field on crack-propagation behavior is shown.

H.P. Rossmanith is associated with Institute of Mechanics, Technical University Vienna, Karlplatz 13, A-1040, Vienna, Austria. A. Shukla (SESA Member) is Assistant Professor, Department of Mechanical Engineering and Applied Mechanics, University of Rhode Island, Kingston, RI 02881.

Paper was presented at Fourth SESA International Congress on Experimental Mechanics held in Boston, MA on May 25-30, 1980.

Original manuscript submitted: August 1, 1980. Authors notified of acceptance: November 5, 1980. Final version received: February 23, 1981.

Theoretical Considerations

When elastic waves are propagated and transmitted during blasting or an earthquake phenomenon, they are diffracted at an obstacle or geometric discontinuity and often give rise to a high elevation of local stresses. These stress concentrations become extremely severe when the static or moving discontinuity is a crack. The result of waves reflecting and refracting at the moving crack tip can lead to undesirable crack-instability behavior. There are two kinds of body waves: The P-wave (also primary, compressional, dilatational, irrotational or longitudinal wave) and the slower S-wave (also secondary, equivoluminal, rotational, shear or transverse wave). The P-wave is polarized in the direction of the incoming wave, while the S-wave can be polarized parallel to the horizontal x-z crack plane (SH-wave) or parallel to the vertical x-y plane (SV-wave) as shown in Fig. 1. Plane dynamic photoelasticity deals with P- and SV-wave propagation.

In fracture mechanics, the deformations of the crack walls induced by the wave motion are classified into three modes: Mode 1 = > normal opening mode deformation; Mode 2 = > in-plane shearing-mode deformation, and Mode 3 = > anti-plane shearing-mode deformation. In connection with (obliquely) impinging P and SV-waves, the first two fracture modes occur in various combinations.

Consider the propagation of elastic waves and their interaction with running cracks as shown in Figs. 2 and 3. The input waves are diffracted and scattered about the moving crack tip. Regardless of the type of incident waves, whether P- or SV-waves, diffraction consists of both P- and SV-waves. Hence, the resulting stress field $\sigma_{ij}(x,y,t)$ is composed of the stress field of the incident wave $\sigma_{ij}^{(i)}(x,y,t)$ and the diffracted P- and SV-waves $\sigma_{ij}^{(s)}(x,y,t)$:

$$\sigma_{ij}(x,y,t) = \sigma_{ij}^{(i)}(x,y,t) + \sigma_{ij}^{(s)}(x,y,t) \qquad (1)$$

where the scattered field $\sigma_{ij}^{(s)}$ must satisfy the condition

$$\sigma_{ij}^{(s)} \to 0 \text{ as } \sqrt{x^2+y^2} \to \infty \qquad (2)$$

If the crack occupies a line L along $y = 0$, the normal

and shear stresses on L are required to vanish such that the boundary conditions are satisfied:

$$\sigma_{ij}^{(i)}(x,o,t) + \sigma_{ij}^{(s)}(x,o,t) = 0, \quad x \notin L$$
$$\sigma_{xy}^{(i)}(x,o,t) + \sigma_{xy}^{(s)}(x,o,t) = 0, \quad x \notin L \tag{3}$$

In the analysis[4] for convenience, the mixed-mode fracture problem is divided into a symmetric part (Mode 1) and an antisymmetric (Mode 2). The corresponding mixed-boundary conditions are:

Mode 1:

$$u_y^{(s)}(x,o,t) = \sigma_{xy}^{(s)}(x,o,t) = 0, \quad x \notin L$$
$$\sigma_{yy}^{(s)}(x,o,t) = -\sigma_{yy}^{(i)}(x,o,t);$$
$$\sigma_{xy}^{(s)}(x,o,t) = 0 \qquad x \in L \tag{4}$$

Mode 2:

$$u_x^{(s)}(x,o,t) = \sigma_{yy}^{(s)}(x,o,t) = 0 \quad x \notin L$$
$$\sigma_{xy}^{(s)}(x,o,t) = -\sigma_{xy}^{(i)}(x,o,t)$$
$$u_{yy}^{(s)}(x,o,t) = 0 \qquad x \in L \tag{5}$$

The solution of the original problem is obtained by superposition of the particular pure-mode solutions.

Figure 2(b) shows the diffraction of a dilatational P-stress pulse impinging at oblique incidence on a plane moving crack. As a result of the wave diffraction, the following zones can be identified during the crack-wave interaction:

I—undisturbed region
II—incident-pulse zone

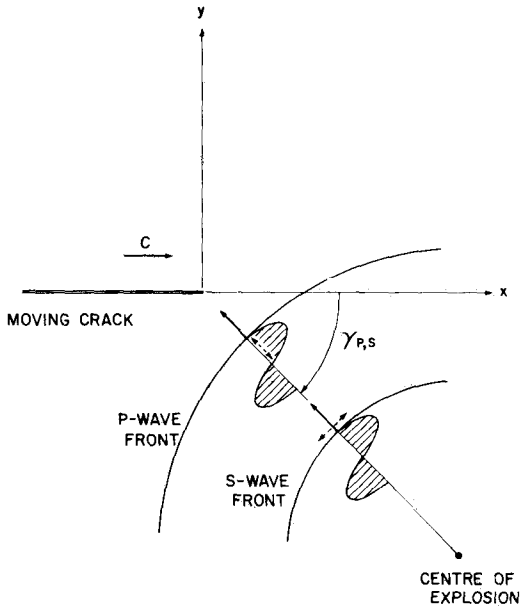

Fig. 1—Position of moving crack and incident elastic P- and SV-waves

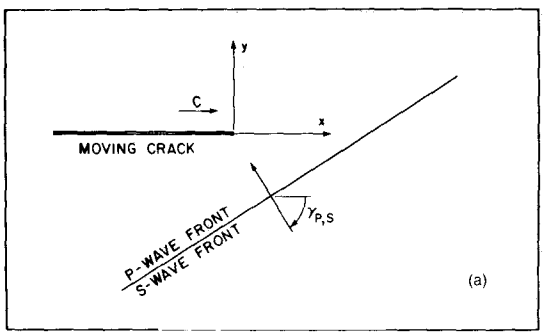

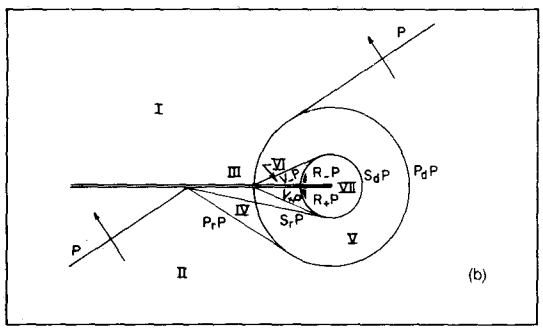

(a) Wave incidence
(b) P-wave scattering

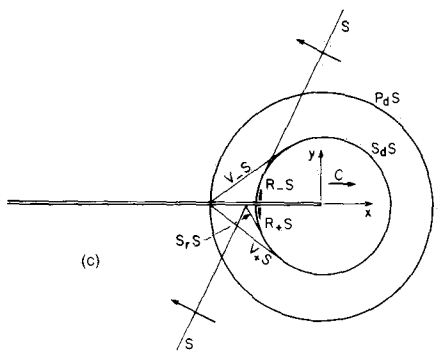

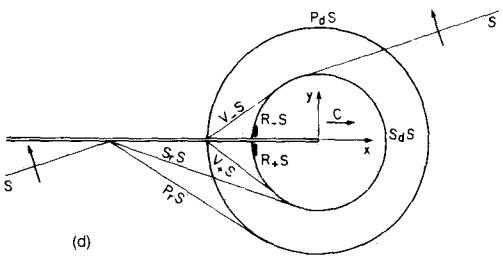

(c) SV-wave scattering (angle of incidence is less than critical angle)
(d) SV-wave scattering (angle of incidence is greater than critical angle)

Fig. 2—Scattering of P- and SV-waves about a moving crack

III—shadow zone
IV—geometric reflection zone
V—dilatational-wave scattering zone
VI—von Schmidt-wave zone
VII—shear-wave scattering zone

The following waves are generated during the course P(SV)-wave diffraction about cracks:

(P_dS, P_dP) diffracted P-wave
(S_dS, S_dP) diffracted S-wave
(P_rS, P_rP) reflected P-wave
(S_rS, S_rP) reflected S-wave
($V \pm S$, $V \pm P$) von Schmidt waves (+ front face, − backface)
($R \pm S$, $R \pm P$) Rayleigh wave

The individual wave types may easily be identified in Fig. 2.

Moving-cracks interacting with P- and SV-waves have been investigated by Chen and Sih.[4] For plane harmonic waves, the treatment for running cracks is similar to the method for stationary cracks except that the problem is formulated with respect to a set of moving coordinates. Wave potentials for the incident wave and the scattered-wave system are then defined which satisfy the Helmholtz equation. The total-wave field for the moving-crack problem may be considered as the linear sum of an incident field and a perturbed field. Satisfaction of the boundary conditions leads to the solution of systems of dual-integral equations and application of the Wiener, Hopf technique. Either input wave, P- or SV-wave, will generate scattered-wave systems containing both P- and SV-wave contributions. Hence, both stress-intensity factors K_1 and K_2 are present in the general case.

The $r^{-1/2}$ stress singularity is the same as that of a stationary crack, while the angular variation of the stress field around the crack tip is increasingly distorted with increasing crack velocity.

The dynamic stress-intensity factors K_1 and K_2 for the moving crack-wave interaction process are complicated functions of the circular frequency ω, input-wave amplitudes σ and τ, angles of incidence γ_p and γ_s and crack speed c. If the influence of input P- and SV-wave in K_1 and K_2 is separated the dynamic-stress-intensity factors for incidence of harmonic P- or SV-waves can be represented in the form:

P-wave incidence,

$$K_p^* \equiv \overline{K}_{p1} - i\overline{K}_{p2} = \sigma\sqrt{\lambda_p}(K_{p1} - iK_{p2})\cos\left[M_p\alpha_p x - \omega\left(\frac{1 + M_p\cos\gamma_p}{S_p^2}t - \frac{T}{8}\right)\right] \tag{6}$$

SV-wave incidence,

$$K_s^* \equiv \overline{K}_{s1} - i\overline{K}_{s2} = \tau\sqrt{\lambda_s}(K_{s1} - iK_{s2})\cos\left[M_s\alpha_s x - \omega\left(\frac{1 + M_s\cos\gamma_s}{S_s^2}t - \frac{T}{8}\right)\right] \tag{7}$$

here $M_j = c/c_j$ are the Mach numbers [c_j . . . longitudinal ($j = p$) and shear ($j = s$) wave velocities],
$S_j = (1 - M_j^2)^{1/2}$,
α_j is a function of the input wavelength, the Mach number and angle of incidence, and T is the period of the input wave.

Assuming, with some reservation, the validity of the classical relation between stress-intensity factors K_j and the energy release rate G also for the present problem, one obtains:

$$G_x(c) = \frac{1 - \nu^2}{E}[A_1(c)K_{x1}^2 + A_2(c)K_{x2}^2] \tag{8}$$

where the functions $A_i(c)$ ($i = 1, 2$) depend only on the Mach numbers M and are defined in Ref. 6, and x stands for p or s.

Numerical results of K_{pj} and K_{sj} ($j = 1, 2$) as a function of γ_p, γ_s, M_p, M_s taken from Ref. 4 are presented in Figs. 3(a)-(d). It can be noted that the peaks of the individual contributions K_{pj} and K_{sj} do not coincide but occur at different angles. This phase difference in $\overline{K}_1$ and $\overline{K}_2$ which depends on the crack speed, angle of incidence, etc., has a significant influence on the crack-path stability under dynamic mixed-mode conditions.

Fig. 3—Qualitative distribution of dynamic-stress-intensity factors for elastic waves obliquely striking a crack moving at different velocities

(a) Normal-stress-intensity factor for P-wave scattering
(b) In-plane shear-stress-intensity factor for P-wave scattering
(c) Normal-stress-intensity factor for SV-wave scattering
(d) In-plane shear-stress-intensity factor for SV-wave scattering

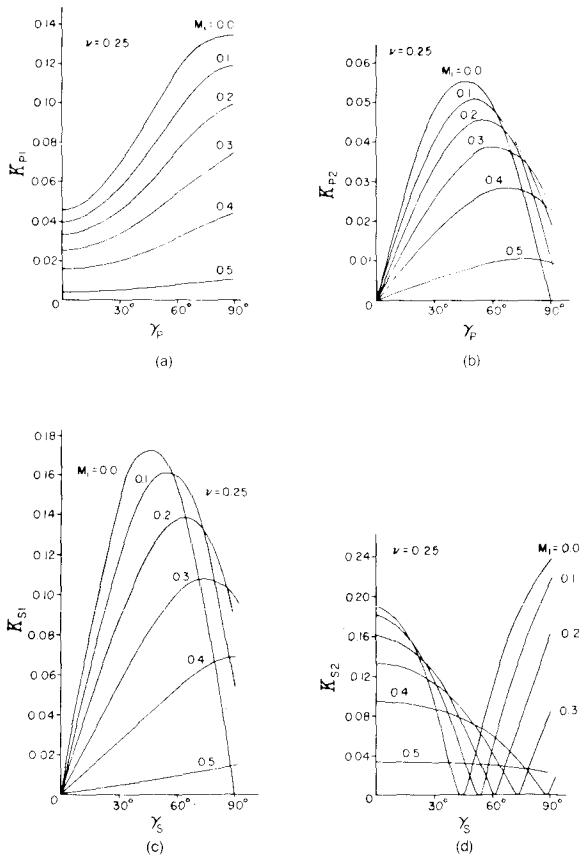

Photoelastic Study of Running-crack-wave Interaction

Experimental Procedure

Dynamic photoelasticity was utilized to study running-

crack-wave interaction in a single-edge-notched specimen. Photoelasticity provides whole-field data during the propagation period which contains the instantaneous stress-intensity factor, crack-tip position and the change in the state of stress across the section due to crack movement and crack-wave interaction.

The geometry of the single-edge-notched specimens used in this study is shown in Fig. 4. The specimens were fabricated from a 9.5-mm-thick sheet of a brittle polyester, Homalite 100. This polyester becomes birefringent when subjected to a state of stress and gives rise to optical-interference fringes when viewed in a circular polariscope. These fringes are known as isochromatics and represent line along which the maximum shear stress is a constant.

A blunt starter crack was saw cut into the specimen as shown in Fig. 4 and the crack tip was rounded to inhibit premature initiation at high values of K_Q. The crack was then initiated by drawing a sharp blade across the tip. As the crack propagated, it interrupted a silver conductive paint line on the model and triggered the multiple-spark Cranz-Schardin camera[7] and the explosive after some prescribed delay time. The Cranz-Schardin camera used provides 16 frames at discrete times during the dynamic event. The sparks provide light pulses about 500 ns in duration and thus effectively stop the motion of the fringes during the exposure time. A framing rate of about 200,000 frames/s was used in the experiments. This provided an observation period of 90 μs which was well matched with the interaction process being studied. Three experiments were conducted with the explosive excitation at positions I, II and III as shown in Fig. 4.

Normal Incidence

A stress wave is said to impinge normally onto a static or running crack when the direction of wave propagation is parallel and opposite to the crack-propagation direction. Normal incidence of and SV-wave on a moving-crack tip

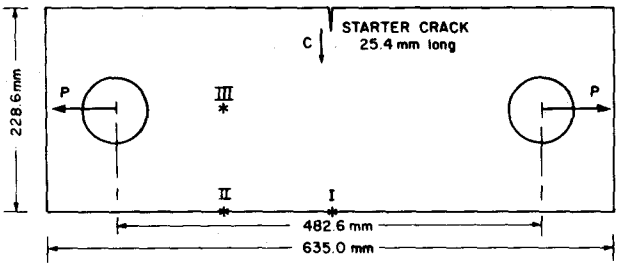

Fig. 4—Geometry of the specimen

and their diffraction is shown in the sequence of photographs of Figs. 5, 6 and 8.

In the first experiment, the explosive was fired at Site I shown in Fig. 4. A P-wave (c_1 = 2150 m/s), an SV-wave (c_2 = 1240 m/s), and trailing bending waves are generated at the explosion site and radiate into the material. At the same time, a high-velocity running crack (c = 380 m/s) is initiated from the starter crack and propagates opposite to the wave-propagation direction. The preinteraction phase between the waves and the crack is shown in Fig. 5. By the time the interaction occurs, the P-wave and S-wave have already separated. P-wave diffraction at the crack tip is depicted in the fringe patterns and wavefront reconstruction shown in Figs. 6(a)-(c) and 7. The fringe pattern presented in Fig. 6(a) shows the mutual far-field interaction as the crack tip normally approaches the P-wave front at time t = 65 μs after initiation of the crack. The crack tip is surrounded by a butterfly isochromatic-fringe pattern which is typical for Mode 1 cracks propagating at nearly terminal velocity (c = 380 m/s) in an SEN specimen characterized by increasing K values as the crack proceeds. When the P-wavefront is scattered at the moving-crack tip both a PP_1-wave and a SP_1 wave are generated by diffraction. During its extension, the P-wave is reflected at the crack wall at grazing incidence, hence producing the so-called von Schmidt waves ($V \pm P_1$) as shown in Fig. 7. The second photograph 6(b) shows the

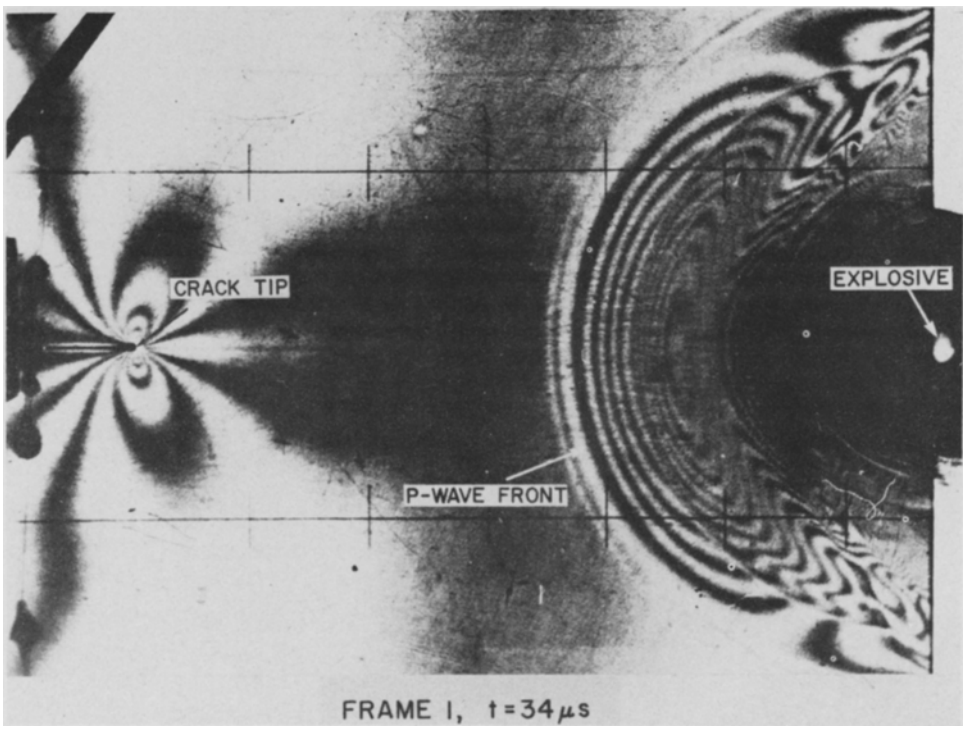

Fig. 5—Preinteraction phase showing the explosive generation of elastic waves and a high-velocity running Mode 1 crack

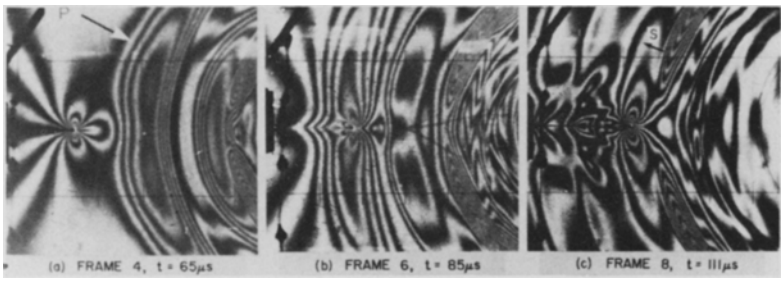

(a) Mutual far-field interaction as the crack tip normally approaches the wavefront
(b) Crack tip traversing the leading compressive pulse of the P-wave
(c) Crack tip traversing the trailing tensile pulse of the P-wave

Fig. 6—Diffraction of a normally incident P-wave about a high-velocity running-crack tip (crack speed, c = 380 m/s; P-wave velocity, c_1 = 2150 m/s) in Homalite 100

phase when the crack tip traverses the peak of the leading compressive pulse of the P-wave (frame t = 85 μs). Notice that the classical butterfly isochromatics have been completely distorted by the transient stress-field component which acts parallel to the crack line. An unstable quadruple-fringe pattern is generated during the passage of the compressive half of the P-pulse.

The final photograph of this sequence depicts the situation where the crack tip traverses the trailing tensile pulse of the P-wave. The strong increase of crack-tip fringe order from N = 5 in Fig. 6(a) to the visible order N = 8 indicates an essential increase of the stress-intensity factor. Despite the favorable biaxial-tensile-stress field associated with the trailing half of the P-wave, crack branching is not to be expected at this early stage of crack propagation because the combination of K and c pertains to the far-left range of the characteristic c–K relationship.[8,9] The wavefront reconstruction associated with scattering of leading half of the P-pulse is illustrated in Fig. 7. Note that the crack moves during impingement of the wave, thus generating complicated scattered-wave patterns. Although corresponding diffracted P- and S-wave parts are concentric about the instantaneous crack-tip position, one notices that the diffracted P- and S-wave systems do not show annulus-shaped forms because of the relative movement of the crack tip between scattering of individual parts of the P-wave.

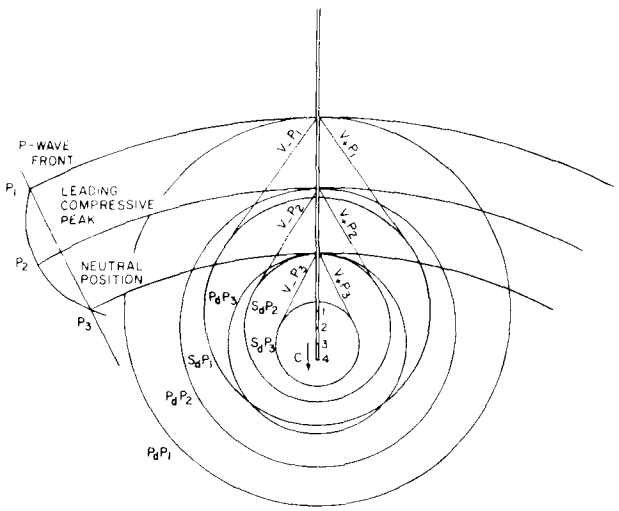

Fig. 7—Wavefront reconstruction associated with P-wave scattering about a fast-running crack. Crack-tip positions 1, 2, 3 and 4 correspond to scattering of P-wavefront, leading compressive peak, neutral position, and actual configuration (Rayleigh-wave generation not presented)

The second sequence of photographs in Fig. 8 shows the diffraction of a normally incident SV-wave about a running-crack tip. Shear waves generated by explosive excitation at the free boundary of the specimen exhibit a line of symmetry which is identical with the normal to the boundary. Little interaction between the SV-wave and the advancing crack is to be expected because the crack penetrates the wavefront along the line of symmetry. This is evident from the visible crack-tip fringe orders in frames 9 and 10 of Fig. 8 which are of the same magnitude (N = 7). Frame 9 (t = 122 μs) shows the crack tip passing the peak line of the SV-wave. In frame 10 (t = 133 μs) the SV-wave has passed the crack tip and trailing bending waves start to interact with the crack to produce weak but complex crack-path irregularities.

Normally incident P-wave scattering about a running-crack tip causes pure opening-mode deformation associated with Mode 1 stress-intensity factor $K_1 \neq 0$ and $K_2 \equiv 0$. This follows also from Fig. 3(a) and (b) for $\gamma_1 = 0$. Moreover, the dynamic-stress-intensity factor decreases with increasing crack speed. The distribution of stress-intensity factor due to normally incident SV-wave scattering is

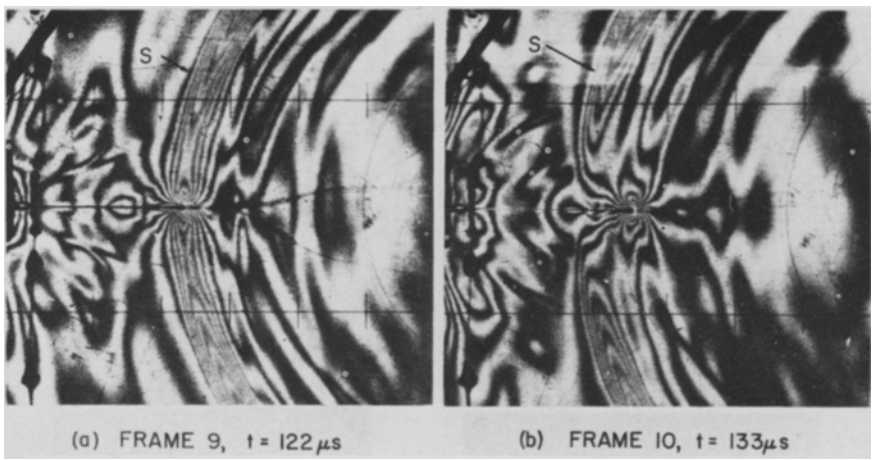

(a) Crack-tip passing peak line of SV-wave
(b) Postpassage phase of SV-wave interaction

Fig. 8—Diffraction of a normally incident SV-wave about a high-velocity running-crack tip

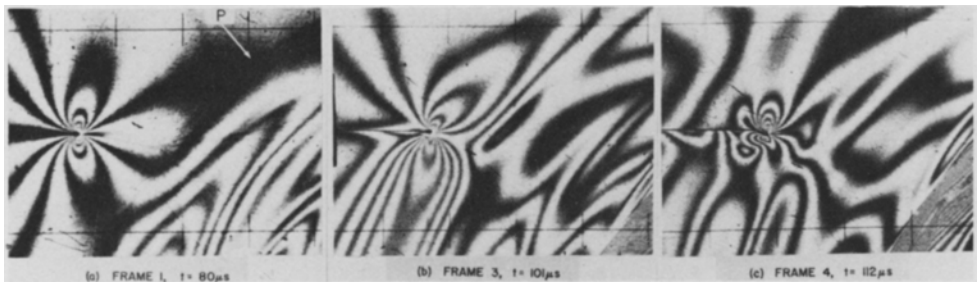

(a) Far-field interaction of moving-crack-tip stress field and incident leading compressive P-wave pulse
(b) Compressive P-pulse generating a dynamic mixed-mode stress pattern around the crack-tip
(c) Dynamic mixed-mode stress field showing crack-path waviness due to P-wave interaction

Fig. 9—Diffraction of an obliquely incident P-wave about a high-velocity running-crack tip (crack speed, c = 380 m/s; P-wave velocity, c_1 = 2150 m/s) in Homalite 100

more complex. Normally, impinging-plane SV-waves give rise to pure shearing-mode deformation at the crack tip, hence $K_I = 0$. Explosively generated cylindrical SV-waves (shown in Fig. 8) possess several axes of symmetry as such the K distributions for plane harmonic SV-waves shown in Figs 3(c)-(d) cannot be applied to explosively generated SV-waves. If, in Fig. 8, the SV-wavefront was rotated at an angle of 45 deg, the crack would interact with the isochromatic peak of the SV-wave which is a position of maximum shear stress, i.e., $\sigma_1 = -\sigma_2$ and $\tau_{max} = \frac{\sigma_1}{2}$. The crack would then be subjected to pure Mode 2 deformation.

Oblique Incidence

A stress wave is said to be obliquely incident onto a moving-crack tip when the angle formed by the normal unit vectors to the wavefront and the crack line differ from zero and 90 deg. During the interaction process, this angle is constant for plane waves but changes when cylindrical waves impinge on the crack.

The sequence of photographs in Fig. 9 shows the diffraction of an obliquely incident P-wave about a high-velocity running-crack tip. Figure 9(a) shows the pre-stressed SEN specimen exhibiting the classical butterfly-shaped isochromatic fringes of visible order $N = 6$. At the same time, the leading compressive pulse of the P-wave radiates from the position II in Fig. 4 with the peak fringe order of 4.75. The ratio of the principal stresses associated with a single compressive cylindrical P-pulse is about $\sigma_r/\sigma_\theta = \sigma_1/\sigma_2 = 2.5$. The P-wave impinges the crack tip at an angle of about 30 deg with respect to the crack line. The wave-induced stress field is superimposed onto the stress field caused due to the loading of the specimen. The stress components of the P-wave can be split into three components which act normal, parallel and tangential to the crack. The normal compressive-stress component gives rise to an opening-mode crack deformation. The stress field acting parallel to the crack line plays an important role in the stability of crack extension, and the tangential stress component causes in-plane shearing deformation of the crack walls.

Analysis of the isochromatic near crack-tip fringe patterns [Figs. 9(a) and 9(b)] on the basis of a static mixed-mode analysis reveals a dominant Mode 1, mixed-mode crack problem with the sign of the transient stress field parallel to the crack line changing from negative [compression in Fig. 9(b)] to positive [tension in Fig. 9(c)]. Note that, in Fig. 9(b), the crack tip deviates from its straight crack path due to the transient-stress-induced mixed-mode situation. The crack-path curvature apparently changes sign between frame 3 [Fig. 9(b)] and frame 4 [Fig. 9(c)]. The geometric features of the resulting wavy crack path may be utilized to determine an apparent mixed-mode ratio function $m(t) = K_{II}/K_I$ of the interaction process.

Oblique SV-wave scattering about a moving crack is depicted in the sequence of photographs shown in Figs. 10(a)-(c). In Fig. 10(a), (frame 7, t = 141 μs) the crack tip is surrounded by nearly pure Mode 1 isochromatic fringes ($N \cong 7$) as the crack approaches the oblique incident SV-wave ($N \cong 10.5$). The angle of incidence is greater than the critical angle and the wave is diffracted at the crack tip [Fig. 10(b)] giving rise to a diffracted- and reflected-wave system. The wavefront reconstruction associated with Fig. 10(c) is similar to the one shown in Fig. 2(d), with the difference that the incident and reflected wavefronts are curved. Note that, unlike the plane wavefronts, the stress intensity will vary along the

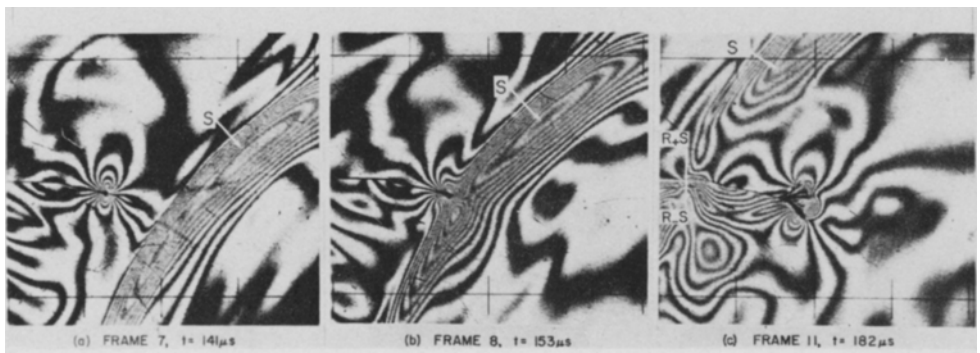

(a) Oblique SV-wave approaching the crack tip
(b) SV-wave scattering about moving-crack tip
(c) Multiple crack branching due to the joint action of SV-wave and reflected tensile P-waves from the specimen boundary

Fig. 10—Diffraction of an obliquely incident SV-wave about a high-velocity crack

cylindrical wavefronts because of the change in angle of incidence as successive elementary length of the wavefront strikes the crack surface. Oblique SV-wave scattering gives rise to apparent mixed-mode stress concentrations at the moving-crack tip. This is also shown in the theoretical results presented in Fig. 3(c)-(d). The SV-wave-induced Mode 1 stress intensity becomes very large and, momentarily, the value of the strain-energy-release rate approaches a critical limit. The crack finally divides into two or eventually several individual branches when the quantity $\mathcal{G}.c$ associated with the system of branches becomes larger than the $\mathcal{G}.c$ value for the single running crack.[9,11]

Tangential Incidence

A stress wave is said to be tangentially incident onto a moving-crack tip when the angle formed by the normal unit vectors to the wavefront and crack line is 90 deg. This angle stays constant for plane waves but changes during the course of interaction for cylindrical waves.

In the third experiment, the explosive is fired at site III and the sequence of pictures in Fig. 11 shows the interaction process. Figure 11(a) shows a high-velocity crack running at right angles to the wave-propagation direction. The near field at the crack tip is not disturbed but interaction does occur in the far field as the P-wave approaches the crack tip. Figure 11(b) shows the impingement of the leading compressive pulse of the P-wave on the crack tip. As the wave passes over the crack tip, the crack adjusts itself to the new state of stress and thus deviates from its stable straight crack path. In the subsequent photographs, the wave system became extremely complicated as the reflected waves from the boundary of the specimen started interacting with the running crack. The effect of this interaction is very profound as crack branching is completely suppressed in the specimen. The crack propagates in a wavy path as shown in Fig. 11(c) and 11(d), with radius of curvature changing sign several times before the crack propagates through the specimen. During the propagation phase, the stress-intensity factor also oscillates as shown by the visible fringe orders at the crack tip. The fringe order changes from $N = 4$ in frame 5 to $N = 7$ in frame 11 and again to $N = 4$ in frame 14.

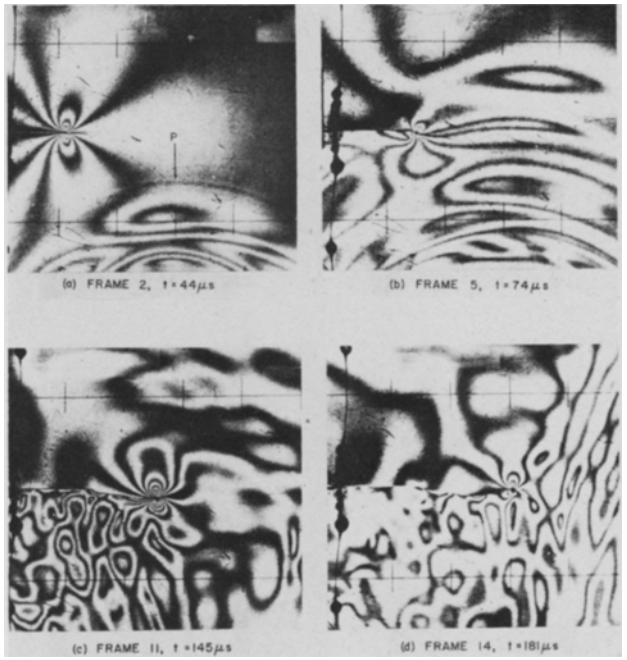

Fig. 11—Diffraction of a tangentially incident wave about a high-speed moving crack

The isochromatic fringes in all the frames appear skewed in the near far field of the crack tip. These fringes appear to become symmetric as one approaches the crack tip. This supports the authors' contention that cracks travel in Mode 1 only and, as such, the fringes should be symmetric in the singularity-dominated zone. Hence, the experimentally recorded photograph of a dynamic mixed-mode propagating crack in Fig. 9(c) shows an apparent dynamic mixed-mode isochromatic crack-tip pattern surrounding a dynamic Mode 1 near crack-tip fringe pattern. The latter fringe system cannot be detected here because the fracture-process zone in the model material is relatively small at the velocities considered. Using this

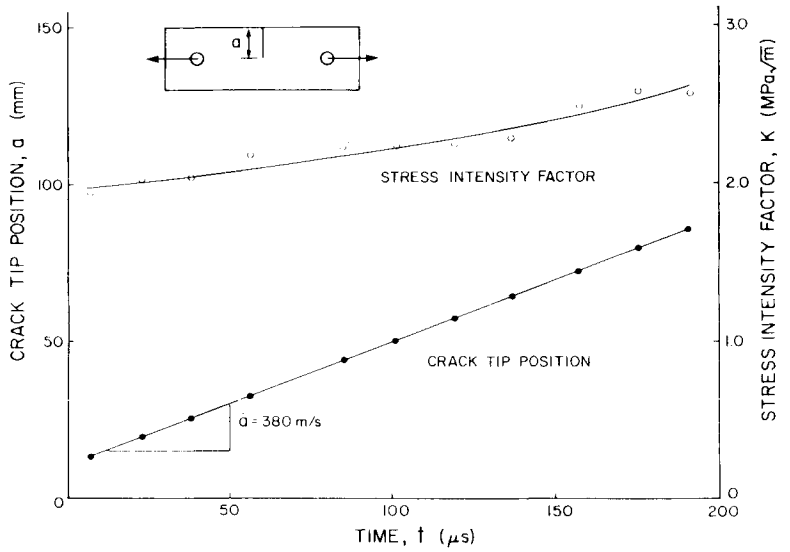

Fig. 12—SEN-CPL (single-edge-notched center-pin loaded) fracture-test specimen, geometry, stress-intensity factor K and crack-tip position a vs. time relationships

fact, one can estimate the size of the singularity-dominated zone which appears to be less than 2 mm in Fig. 11(d) for the specimen at the instant.

Conclusion and Discussion

Dynamic photoelasticity was employed to provide 'whole-field' data for stress-wave scattering about moving-crack tips in prestressed SEN-fracture test specimens. The isochromatic data were analyzed to identify the diffracted and reflected body waves and Rayleigh waves. A qualitative estimate of the stress intensity at the crack tip was also made.

P-waves impinging normally on the moving crack give rise to Mode I type crack deformation. The associated stress-intensity factor K_I caused by static preload of the specimen is lowered during the passage of the leading compressive pulse of the P-wave, but K_I increases when the trailing tensile P-pulse passes over the crack tip. The energy content of the trailing tensile pulse is low as such crack branching is not to be expected provided the crack moves in the first half of the specimen. The characteristic K vs. a/w relation for the SEN specimen is shown in Fig. 12 where a/w denotes the ratio of the crack length to the width of the specimen. The dashed line in Fig. 13 represents the influence of the P-wave diffraction on the value of K. Delayed (enhanced) crack branching occurs when the crack meets with the normally impinging leading compressive (trailing tensile) pulse in the second half of the SEN specimen ($a/w > 0.5$), where the preload stress-intensity factor is close to its critical value for branching.

Oblique-incident SV-wave scattering causes transient apparent-mixed-mode stress field which, in turn, causes the crack to deviate from its originally stable straight crack path.[12] Finally, crack branching is possible for oblique SV-wave-crack interaction.

Fracture specimens from each experiment were examined and the position of crack branching noted. The results are presented in Table 1. It is interesting to note that crack branching is enhanced in the case of normal and oblique incidence. The result of tangential incidence is baffling and might have been influenced by unloading effects in the specimen due to borehole cracking.

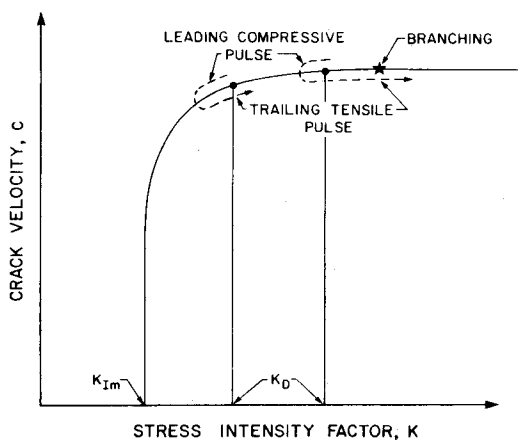

Fig. 13—Crack velocity vs. stress-intensity-factor relationship showing delay and enhancement of crack branching due to leading compressive and trailing-tensile-stress pulses, respectively, of a P-wave scattered about a moving-crack tip

TABLE 1—INFLUENCE OF STRESS WAVES ON CRACK-BRANCHING POSITION

Experiment	K_Q*, MPa $\sqrt{m}$	Position of Crack Branching, a/w
Normal Incidence	1.49	0.45
Oblique Incidence	1.49	0.40
Tangential Incidence	1.49	No Branching
No Stress Waves	1.82	0.68

*Stress-intensity factor associated with initial blunt crack tip.

The authors wish to emphasize the qualitative rather than the quantitative nature of the results. At present, data-reduction methods for the determination of stress-intensity factors associated with transient and gradient stress fields are not developed. On the other hand, analytical results are restricted to the class of basic problems which can be treated numerically. However, despite the number of assumptions made, the comparison of test results with the analytical results of Chen and Sih[4] are surprisingly favorable even though the wave forms are quite different.

Acknowledgment

The authors were supported in this research program by the National Science Foundation under Contract No. DAR-77-05171 and the Photomechanics Lab of the University of Maryland.

References

1. Achenbach, J.D., *Wave propagation in elastic solids*, North-Holland Co., Amsterdam (1973).

2. Ewing, W.M., Jardesky, W.S. and Press, F., *Elastic Waves in Layered Media*, McGraw-Hill, New York (1957).

3. Rinehart, J.S., *Stress Transients in Solids, Hyperdynamics*, Santa Fe, NM (1975).

4. Chen, P.E. and Sih, G.C., Chapt. 1 and 3 of "Elastodynamic Crack Problems" in *Mechanics of Fracture 4* (ed. by G.C. Sih), Noordhof Int. Publ., Leyden (1977).

5. Smith, D.G., "A Photoelastic Investigation of Stress-wave Loading of a Crack," *SESA Spring Meeting 1971*, Salt Lake City, Utah.

6. Freund, L.B., "Crack Propagation in an Elastic Solid Subjected to General Loading - IV. Obliquely Incident Stress Pulse," *J. Mech. Phys. Solids*, **22**, 137-146 (1974).

7. Cranz, C. and Schardin, H., *Zeits. f. Phys.*, **56**, 147-183 (1929).

8. Irwin, G.R., Dally, J.W., Kobayashi, T., Fourney, W.L., Etheridge, M.J. and Rossmanith, H.P., "On the Determination of the $\hat{a}$-K Relationship for Birefringent Polymers," EXPERIMENTAL MECHANICS, **19** (4), 121-128 (1979).

9. Rossmanith, H.P. and Irwin, G.R., "Analysis of Dynamic Isochromatic Crack-Tip Stress Patterns," *Univ. of Maryland Report, 443* (July 1979).

10. Rossmanith, H.P., "Analysis of Mixed-Mode Isochromatic Crack-tip Fringe Patterns," *Acta Mechanica*, **34**, 1-38 (1979).

11. Rossmanith, H.P., "Fringe Loop Dynamics and Crack Branching," in *Proc. of IUTAM-Symposium on Optical Methods in Mechanics of Solids*, Poiters (Sept. 10-14, 1979).

12. Rossmanith, H.P., "Crack Propagation and Branching," in *Proc. of Int. Symp. on the Strain Energy Density Criterion in Memory of the Late Prof. Laszlo Gillemot*, Budapest, Hungary (Sept. 17-19, 1980).